energies

Article

Effect of Connection Resistance between Cyclones and Backpass on Furnace Solids Suspension Density Profile and Circulation Rates in CFB

Guanwen Luo [1], Leming Cheng [1,*], Liyao Li [1], Junfeng Wang [2], Xiaoguo Jiang [2] and Weiguo Zhang [1]

[1] State Key Laboratory of Clean Energy Utilization, Institute for Thermal Power Engineering, Zhejiang University, Hangzhou 310027, China; gwluo@zju.edu.cn (G.L.); liyao_li@zju.edu.cn (L.L.); zwg121@zju.edu.cn (W.Z.)
[2] Harbin Boiler Company Limited, Harbin 150046, China; wangjfeng@hbc.com.cn (J.W.); jiangxg@hbc.com.cn (X.J.)
* Correspondence: lemingc@zju.edu.cn

Citation: Luo, G.; Cheng, L.; Li, L.; Wang, J.; Jiang, X.; Zhang, W. Effect of Connection Resistance between Cyclones and Backpass on Furnace Solids Suspension Density Profile and Circulation Rates in CFB. *Energies* **2021**, *14*, 6162. https://doi.org/10.3390/en14196162

Academic Editors: Artur Blaszczuk, Hairui Yang, Franz Winter and Rafał Kobyłeck

Received: 20 August 2021
Accepted: 21 September 2021
Published: 27 September 2021

Abstract: The connection section between cyclones and backpass is an important configuration in multi-cyclone circulating fluidized bed boilers (CFB). In this work, the resistance coefficient of different connection modes, and connection resistance distribution from each cyclone outlet to backpass (connection branch) in one mode are defined and calculated, in order to investigate their effects on furnace solids suspension density distribution and circulation rates. Three connection modes with different overall resistance coefficients were tested experimentally and analyzed by a 1.5-dimensional model in a four-cyclone scaling CFB apparatus. Both experimental and theoretical results show that, with larger overall resistance of a connection, there are more solids suspended in the furnace bottom and fewer in the top section. The investigation of the C-type connection has revealed that when the branch resistance of the connection decreases from branch No. 1–4, the solids suspension density and circulation rate from corresponding solids recycle loops (No. 1–4) increase. Moreover, the non-uniformity of connection branch resistance distribution will lead to uneven lateral solids suspension density distribution and circulation rates allocation. This effect is enhanced by growing superficial velocity.

Keywords: CFB; connection between cyclones and backpass; resistance; theoretical model; solids suspension density; solids circulation rate

1. Introduction

Circulating fluidized bed boilers have been widely utilized in the industry due to their high combustion efficiency, low emission, and fuel adaptability. As the boiler's capacity increased, the furnace size becomes larger, and more cyclones with solid recycle systems are applied. However, the distributions of solids suspension density on the cross-section in the furnace and solids circulation rates under each cyclone become more non-uniform. This will lead to an uneven temperature profile in a CFB furnace and then cause operation problems.

Previous studies have been conducted towards gas-solid hydrodynamics uniformity in a CFB with multiple cyclones. Results show operating conditions [1–7] and geometric factors [6–11] have influences on furnace solids suspension density and circulation rates distribution among cyclones. However, it was reported that the connection between cyclones and backpass might also have an effect. As some close research, Zhou et al. [1] indicated the non-uniform distributions of cyclone pressure drop in a symmetric six-cyclone CFB cold test rig, that the pressure drops of three cyclones implemented at the one side are 30–50 Pa greater than the cyclones in the other side. They attributed this effect to unequal length of connection ducts from cyclones to backpass at each side, leading to different resistance of connection ducts from both sides. Similarly, Song et al. [12] also discovered the better solid flow uniformity of three circulation loops on one side than another three loops in a six-cyclone 600 MW CFB boiler. And they further put forward that the different connection resistance at each side might result in this. In addition, Mo et al. [13] reported the higher ash temperature and lower circulation rate in the solid recycle loops, if they were located further to the backpass in a multi-cyclone CFB boiler. With pressure equilibrium analysis, they proposed the reason is those solid recycle loops have larger resistance from cyclone outlet to backpass compare to other loops.

As the studies indicated above, the connection between cyclones and backpass has a potential impact on solids suspension profile in furnace and circulation rates distribution in a CFB. The connection resistance and resistance distribution from each cyclone outlet to backpass (connection branch) are reported essential to this. However, detailed studies on connection resistance and resistance distribution among connection branches are lacking. And their effect on furnace solids suspension density and circulation rates distribution in a CFB also remain unknown.

For those reasons, this article focuses on the connection between cyclones and backpass, to investigate the effect of connection resistance on furnace solids suspension density and solids circulation rates in a CFB.

Firstly, a four-cyclone scaling CFB model with measuring techniques is introduced in this article. Then, the definition and calculation of branch resistance in a connection, and overall resistance of A, B, and C-type connection modes are presented. To step further, a 1.5-dimentional theoretical model based on mass and pressure equilibrium is established to analyze the relationship among connection resistance, solids suspension density distribution, and solids circulation rates. After experimental system description and theoretical analysis, the results of solids suspension density and solids circulation rates with different connection modes of overall resistance are presented. Besides, this work also focuses on a particular connection mode (C-type mode) to explore the impact of resistance distribution among connection branches, so that the relationship among connection branch resistance distribution, furnace solids suspension density, and circulation rates allocation among four solids recycle loops will be discovered. Eventually, the influence of superficial velocity on furnace suspension density profile and solids circulation rates under different connections is investigated, with *Fn* conditions of 85.2, 91.4, 96.3, and 102.5.

2. Experimental Setup

2.1. Basic Information of the CFB Test Rig

The experiment was conducted on a CFB cold test rig (shown in Figure 1a). It consists of a furnace, four cyclones, solids recycle systems and a connection to the backpass. The bed solids were fluidized by primary and secondary air in the furnace and then entered the cyclones. The air exited from the cyclone outlets passes through the connection section to the backpass, then finally escapes to the atmosphere. Those solids collected by the cyclones return to the furnace via the solids recycle system.

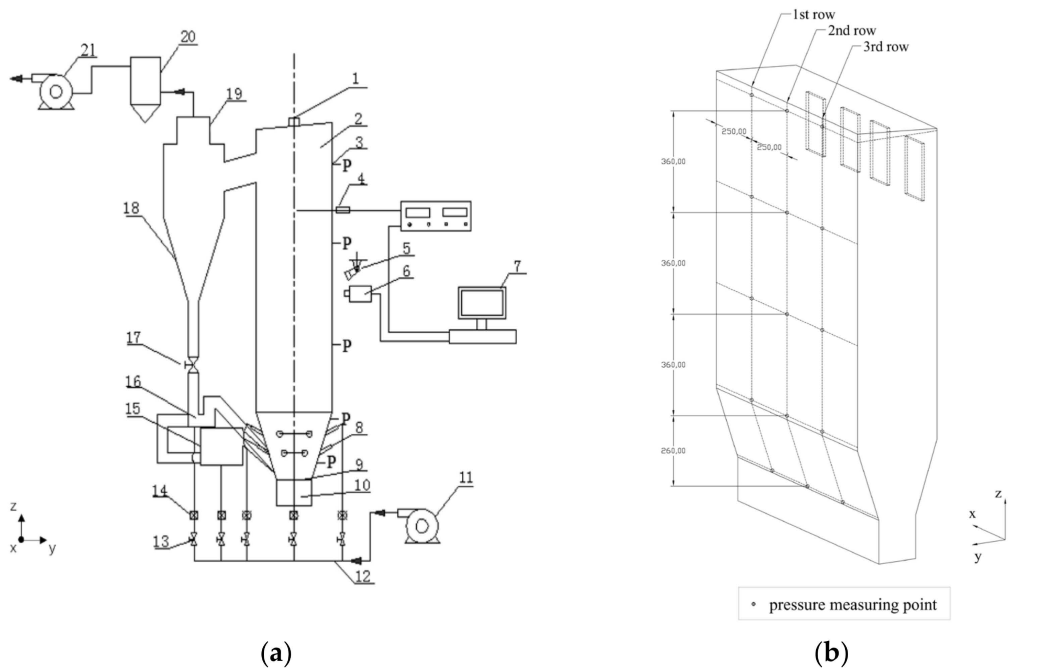

Figure 1. Schematic diagram and pressure measuring points of test rig: (**a**) schematic diagram of experiment. 1-bed material feeder, 2-furnace, 3-pressure taps, 4-pressure transmitter, 5-light, 6-high speed camera, 7-PC, 8-secondary air inlet, 9-distributor, 10-wind chamber, 11-input gas, 12-input gas duct, 13-ball valve, 14-rotameter, 15-External Heat Exchanger, 16-loop-seal, 17-cut off valve, 18-cyclone, 19-connection to the backpass, 20-dust collector, 21-induced draft fan; (**b**) furnace pressure measuring points.

The geometric, operating, and bed material parameters are determined by a simplified fluid dynamic scaling rule [14] based on a 660 MW supercritical CFB boiler. In the simplified Glicksman scaling law, a set of dimensionless groups are derived from governing equations of motion and mass. The dimensionless parameters are identified as:

$$\frac{u_g^2}{gL}, \frac{u_g}{u_{mf}}, \frac{G_{sf}}{\rho_s u_g}, \frac{D}{L}, \Phi, PSD \tag{1}$$

whereas u_g and u_{mf} are superficial velocity and minimum fluidized velocity respectively; L and D are the length and width of the furnace; G_{sf} is solids flux at furnace and ρ_s is solid density; The Φ is the sphericity of the particle; PSD is particle size distribution.

It needs to be noticed that only when particle Reynolds number Re_p in the model is equal to or less than 4, the simplified scaling law can be used [15].

Based on Glicksman scaling law, the geometric structure of the testing model is scaled down by 1:40 from the original CFB boiler. Besides, the operating parameters of the cold apparatus are designed and calculated. Table 1 gives the basic geometric parameters, operating conditions, bed material properties, and dimensionless numbers of both the original boiler and cold model. As shown in the table, all the dimensionless numbers between the cold model and the original boiler are nearly equaled. In addition, the particle Reynolds number in the cold model is close to 4, which corresponds to the viscous limit condition for the simplified Glicksman scaling law.

Table 1. Scaling parameters of original boiler and cold model.

	Items	Symbols	Units	Values in Original Boiler	Values in Test Model
Geometric parameters	Height of furnace	H	m	55.8	1.39
	Length of furnace	L	m	39.95	0.99
	Width of furnace	D	m	12.67	0.32
	Diameter of cyclone	d_c	m	11.20	0.28
	Diamter of standpipe	d_s	m	2.12	0.053
	cross-section of the non-mechanical valve	A_{dis}	m^2	4.84	0.0030
Operating conditions	Temperature	T	°C	880	25
	superficial velocity	u_g	m/s	4.37–5.26	0.69–0.83
	Air velocity in supply chamber	u_{vs}	m/s	–	0.063
	Air velocity in recycle chamber	u_{vr}	m/s	–	0.19–0.38
	Kinematic viscosity	ν	Pa·s	1.51×10^{-4}	1.55×10^{-5}
	Air density	ρ_f	kg/m^3	0.301	1.185
	Solids flux at furnace	G_{sf}	kg/m^2s	16.56	3.14
	Solids flux at a standpipe	G_{sp}	kg/m^2s	678.96	128.74
Bed material properties	Solid diameter	d_p	um	400	94
	Sphericity	Φ	\	0.8	0.8
	Minimum fluidized velocity	u_{mf}	m/s	0.052	0.0081
	Terminal velocity	u_t	m/s	2.91	0.66
	Particle Reynolds number	Re_p	\	11.13	4.02
	Solid density	ρ_s	kg/m^3	2000	2330
Dimensionless numbers	$u_g{}^2/gL$		\	0.069	0.070
	D/L		\	0.317	0.320
	u_g/u_{mf}		\	102.08	102.11
	$G_{sf}/\rho_s u_g$		\	1.57×10^{-3}	1.57×10^{-3}

2.2. Measurement Techniques

The solids suspension density in the furnace was determined by the pressure drop. As shown in Figure 1b, there are three vertical rows of pressure measuring points along the bed length and 5 points in each row along with the bed height. The pressure taps were used to measure the furnace pressure profile. And solids suspension density ρ_{sus} is calculated as

$$\rho_{sus} = \frac{\Delta P}{g\Delta H} \tag{2}$$

where ΔP is the pressure drop between two axial measuring positions with a distance of ΔH. And g is gravitational acceleration with 9.81 m/s^2.

The solids circulation rate was measured at standpipe. Two methods were used to determine the solids circulation rate. The first one is measuring the height of the accumulating solid by cutting off the solids returning flow in the return leg within a specific time. The calculating solids circulation rate at standpipe "i" (i = 1–4) is expressed as,

$$G_{sp,i} = \frac{\rho_s \left(1 - \varepsilon_{mf}\right) h_s}{t_s} \tag{3}$$

where h_s are the solids accumulating height within the specific time t_s.

Another methodology is particle tracking using a high-speed camera to trace the moving particles in the standpipe. The camera for tracking particles is HG-100K high-speed digital camera (REDLAKE company, New Hampshire, USA), with a resolution of 1154 × 1128 and a frame rate (fps) of 125. The colored particles with similar density and diameter to bed material were used as tracer particles. For this method, the solids circulation rate at the standpipe "i" can be calculated as

$$G_{sp,i} = \rho_s \frac{s}{t} \tag{4}$$

where s is the falling distance of tracer particle within specific time t. Figure 2 shows several successive frames of the capturing procedure. To ensure the accuracy of measuring, two or more colored particles with a similar relative location in each frame were treated as valid particles. And up to 1000 frames were used in total to measure and calculate $G_{sp,i}$ at each operating condition.

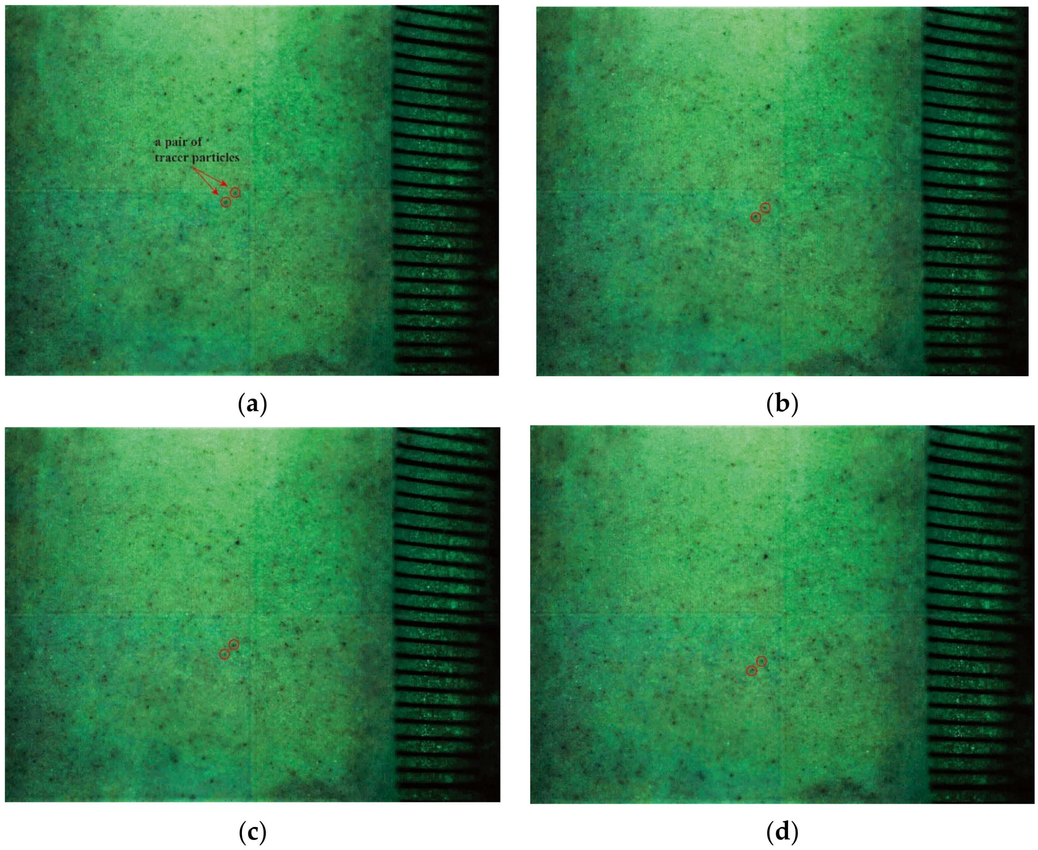

Figure 2. The successive frames of tracer particles are captured by a high-speed camera: (**a**) 1st frame; (**b**) 2nd frame; (**c**) 3rd frame; (**d**) 4th frame.

3. Three Connection Modes and Calculation of Connection Resistance

Three connection modes were tested in the cold apparatus as given in Figure 3. The overall resistance coefficients of each connection mode (ξ_{av}) were calculated based on the Handbook of Hydraulic Resistance [16]. They were determined by averaging the resistance coefficient of the four connection branches ($\xi_{b,i}$).

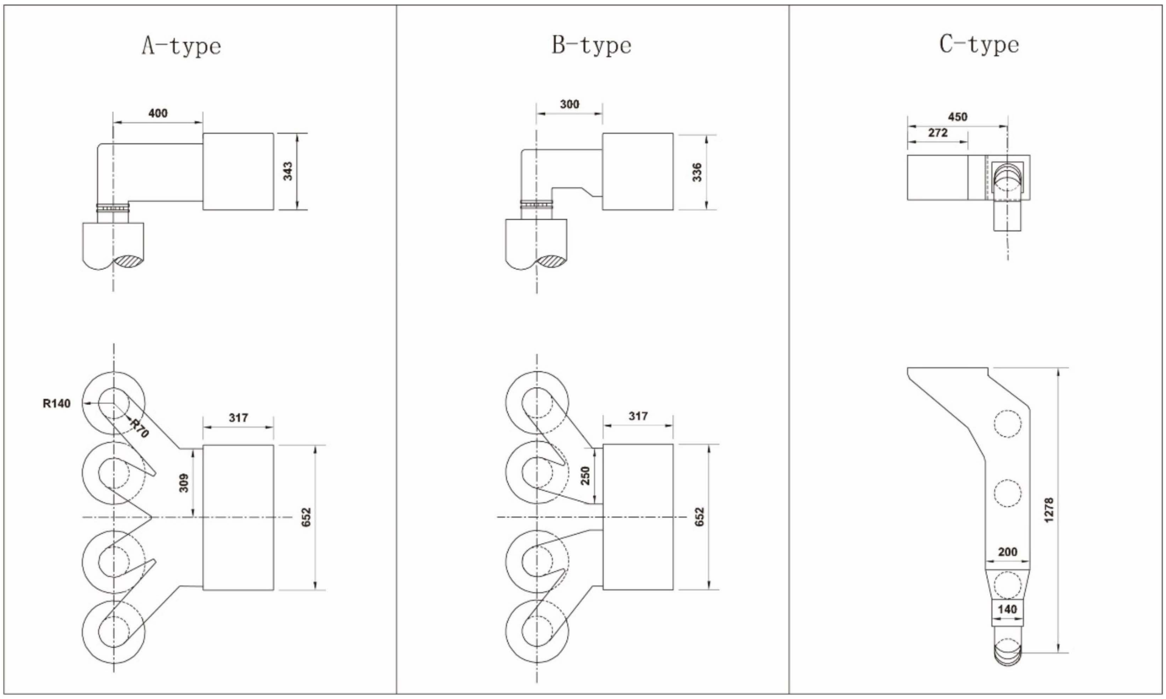

Figure 3. Three testing connection modes.

3.1. Resistance Coefficient of Each Connection Branch of a Connection Mode

The CFB system has four parallel cyclones, and the gas escaped from each cyclone outlet enters the connection section. Therefore, the connection section consists of four branches, starting from each cyclone outlet to the end of the connection, as illustrated in Figure 4. The resistance coefficient of a connection branch ($\xi_{b,i}$, i = 1–4) is calculated by summing the friction resistance coefficient along the path ($\xi_{fr,i}$) and local resistance coefficients ($\xi_{l,i}$) such as a sudden variation of cross-section area. The expression is given by,

$$\xi_{b,i} = \xi_{fr,i} + \xi_{l,i} \ (\mathrm{i} = 1\text{–}4) \tag{5}$$

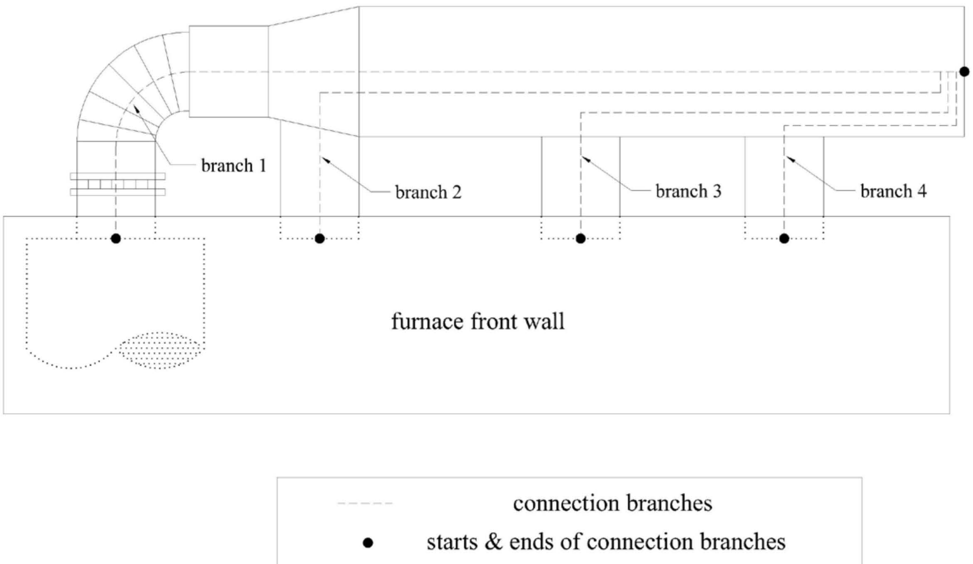

Figure 4. Structure of C-type connection mode (from the view of furnace front wall).

For a connection branch i, the friction resistance coefficient can be expressed as,

$$\xi_{fr,i} = \lambda \sum \frac{l}{D_h} \quad (6)$$

where λ refers to friction coefficient constant, l and D_h are the lengths and hydraulic diameter of the branch path, while the sections along the path might have different D_h.

$\xi_{l,i}$ is the local resistance coefficient, which is mainly decided by geometric parameters. According to Figure 4, taking branch 1 of the C-type connection as an example, the local resistance from the beginning to the end of this branch consists of an elbow, sudden expansion, tees junction, smooth variation, and horizontal band.

The frictional and local resistance coefficients of, A, B, and C-type modes are listed in Table 2. It is noted that the branches 1–4 of, A, B, and C-type are numbered based on cyclones' positions from left to right from the view the of furnace front wall, as hinted in Figure 4. Therefore, concerning symmetric structure of A and B-type connection modes, the connection resistance coefficient of branches 1 and 4, 2 and 3 of both A and B-type connections are equaled, respectively.

Table 2. Resistance coefficient calculation.

Connection Mode	Connection Branch (i)	$\xi_{fr,i}$	$\xi_{l,i}$	Detailed of Local Resistance	$\xi_{b,i}$	ξ_{av}
A-type	1 and 4	0.13	1.51	Elbow with right angle, conjunction wye with angle, sudden expansion*2	1.64	1.58
	2 and 3	0.09	1.43	Elbow with right angle, conjunction wye with angle, sudden expansion*2	1.52	
B-type	1 and 4	0.12	1.60	Elbow with right angle, conjunction wye with angle, sudden expansion*2, smooth expansion	1.82	1.70
	2 and 3	0.09	1.49	Elbow with right angle, conjunction wye with angle, sudden expansion*2, smooth expansion	1.58	
C-type	1	0.16	3.10	elbow, sudden expansion, tee (after junction) *3, smooth expansion, horizontal elbow with sharp corner	3.26	2.89
	2	0.12	2.98	Tee before junction, tee after junction*2, smooth expansion, horizontal elbow with sharp corner	3.10	
	3	0.08	2.66	Tee before junction, tee after junction, smooth expansion, horizontal elbow with sharp corner	2.74	
	4	0.06	1.96	tees before junction and horizontal elbow with sharp corner	2.02	

3.2. Overall Resistance Coefficient of a Connection Mode

For each type of connection mode, the connection section is divided into four parallel branches. Therefore, the overall resistance coefficient of a connection mode can be determined by averaging four branch resistance coefficients,

$$\xi_{av} = \frac{1}{4} \sum_{i=1}^{4} \xi_{b,i} \quad (7)$$

As given in Table 2, the overall resistance coefficient of A, B, and C type connection modes are 1.58, 1.70, and 2.89 respectively. Other details about connection branch resistances are also given in Table 2.

4. Theoretical Analysis

In order to analyze the effect of the connection resistance on solids suspension density in furnace and solids circulation rates distribution theoretically, a 1.5-dimension model based on mass and pressure balance of the CFB system is deduced.

4.1. Solids Recycle Loops and Gas-Flowing Branches

Solids recycle loop and gas-flowing branch in multi-cyclone CFB are defined in Figure 5. The furnace's cross-section is divided into four sections along the bed width, corresponding to four solids recycle systems. A divided furnace section, cyclone, and solids recycle system constitute one of the solids recycle loops (A-B-C-D-A). Similarly, the divided furnace section, cyclone, and connection branch (A-B-E-F) compose a gas-flowing branch, as shown in Figure 5. In the theoretical model, it is assumed gas-solid lateral interactions in the furnace upper section can be ignored, and solids lateral dispersion in the bottom dense section is counted [17].

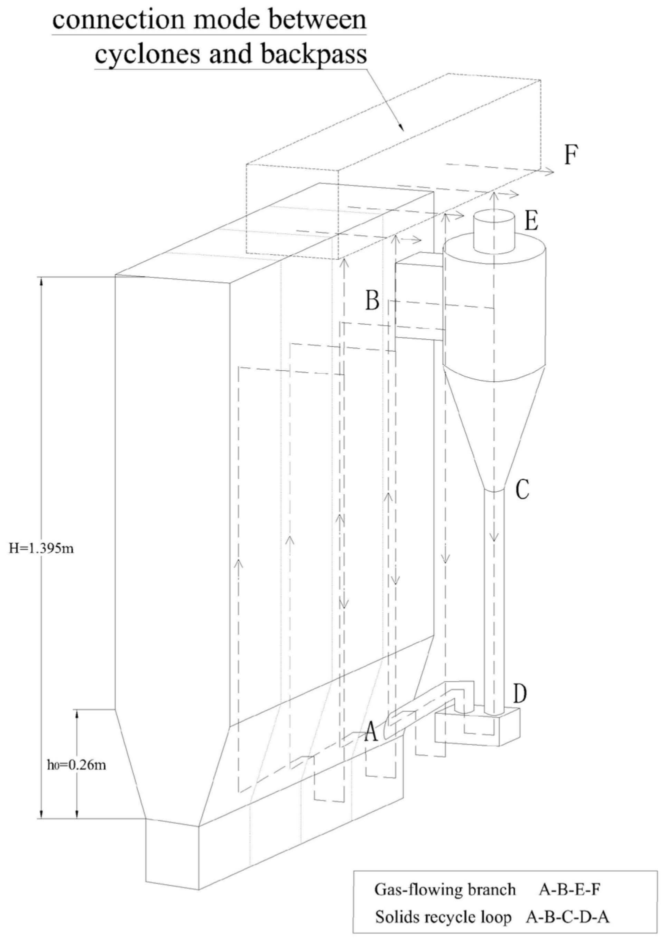

Figure 5. Diagram of gas-flowing branch and solids recycle loop.

For the reason of much narrower cross-section in a divided furnace, some researches regarding CFB riser are considered reasonable here. And each gas-flowing branch or solids recycle loop is denoted by subscript "*i*" in the following theoretical analysis.

4.2. Pressure Drops from Furnace to Each Connection Branch

For branch A-B-E-F, the pressure drop relationship is expressed by the following equation,

$$\Delta P_{AF,i} = \Delta P_{AB,i} + \Delta P_{BE,i} + \Delta P_{EF,i} \tag{8}$$

where $\Delta P_{AB,i}$, $\Delta P_{BE,i}$ and $\Delta P_{EF,i}$ are the pressure drops across the furnace, cyclone, and the connection branch respectively. Since the primary air is evenly distributed above the distributor, $\Delta P_{AF,i}$ is identical for all four gas-flowing branches.

$\Delta P_{AB,i}$ can be obtained as following [18],

$$\Delta P_{AB,i} = \rho_{av,i} g (H - h_0) + \rho_{a,i} g h_0 \tag{9}$$

where $\rho_{a,i}$ refers to solids suspension density in the bottom dense region with a height of h_0. $\rho_{av,i}$ refers to axial average solids suspension density above h_0. The dense region height h_0 was taken approximately as 0.26 m.

The pressure drop across the cyclone is estimated by Equation (10) [19]:

$$\Delta P_{BE,i} = \frac{1}{2}\left(\frac{16A_c}{D_e^2}\right)\rho_g u_{gc,i}^2 \tag{10}$$

where A_c, D_e and $u_{gc,i}$ represent the cross-section area, hydraulic diameter, and gas velocity at the cyclone entrance, respectively.

Pressure drop across a connection branch $\Delta P_{EF,i}$ can be calculated by,

$$\Delta P_{EF,i} = \frac{1}{2}\xi_{b,i}\rho_g u_{go,i}^2 \tag{11}$$

where $u_{go,i}$ is the equivalent gas velocity in a specific connection branch, $\xi_{b,i}$ represents the resistance coefficient of a connection branch calculated by Equation (5) in the previous section.

4.3. Pressure Drops in a Solids Recycle Loop

The sum of pressure drops of solids recycles loop is zero when the system operates steadily. It can be written as,

$$\Delta P_{AB,i} + \Delta P_{BC,i} + \Delta P_{CD,i} + \Delta P_{DA,i} = 0 \tag{12}$$

where $\Delta P_{AB,i}$, $\Delta P_{BC,i}$, $\Delta P_{CD,i}$ and $\Delta P_{DA,i}$ are the pressure drops across furnace, cyclone, standpipe, and loop-seal, respectively.

Here $\Delta P_{AB,i}$ and $\Delta P_{BC,i}$ are calculated according to Equations (9) and (10), respectively [20,21]. The pressure drop $\Delta P_{CD,i}$ in the standpipe of is calculated neglecting solids frictional or acceleration losses in standpipe [21]. It can be given,

$$\Delta P_{CD,i} = \rho_s \left(1 - \varepsilon_{mf}\right) g L_i \tag{13}$$

here L_i is solids stacking height in a standpipe.

The pressure drop across the non-mechanical valve can be written as [22],

$$\Delta P_{DA,i} = \frac{1}{2\rho_s\left(1 - \varepsilon_{mf}\right)}\left(\frac{G_{sp,i}A_{sp}}{C_d A_{dis}\varnothing}\right)^2 \tag{14}$$

where A_{dis} is the vertical cross-section of the non-mechanical valve, $\varnothing$ is sphericity of the particle and C_d is a discharge coefficient about 0.7–0.8 for all kinds of systems and a mid-value of 0.75 was adopted.

4.4. Mass Balance of the Loop in the Whole System

Neglected the solids escaping from the cyclones, the solids mass is balanced in the CFB systems as following,

$$M = M_{sp} + M_f + M_{cyc} \tag{15}$$

where M is the total inventory in the system, which is 25 kg in this study. M_{sp}, M_f and M_{cyc} are the mass of solids in standpipes, furnace, and cyclones respectively. They can be written as following equations,

$$M_{sp} = \rho_s \left(1 - \varepsilon_{mf}\right) A_{sp} \sum_{i=1}^{4} L_i \tag{16}$$

$$\begin{aligned} M_f &= \left(\sum_{i=1}^{4} \rho_{a,i}\right) A_{fb} h_0 + \left(\sum_{i=1}^{4} \rho_{av,i}\right) A_{fd} (H - h_0) \\ &= \overline{\rho}_a A_{fb} h_0 + \left(\sum_{i=1}^{4} \rho_{av,i}\right) A_{fd} (H - h_0) \end{aligned} \tag{17}$$

$$M_{cyc} = k \sum_{i=1}^{4} \rho_{e,i} \tag{18}$$

where A_{fb}, A_{fd} and A_{sp} are the cross-section area of furnace bottom, furnace above dense phase and standpipe, respectively; M_{cyc} is calculated on the assumption that the solids concentration in the cyclone is the linear function to that of the dilute phase at the furnace exit [13]; $\rho_{e,i}$ is the solids suspension density at each furnace exit; $\overline{\rho}_a$ is the average solids suspension density at furnace bottom zone.

4.5. Solids Suspension Density Distribution in the Furnace

For each solids recycle loop, the axial solids suspension density above the dense region can be calculated by Kunii-Levenspiel Equation [23],

$$\frac{\rho_{d,i} - \rho_i}{\rho_{d,i} - \rho_{a,i}} = Exp[-a_{\varepsilon,i}(h - h_0)] \tag{19}$$

where $a_{\varepsilon,i}$ is an axial attenuate coefficient, with the relationship of $a_{\varepsilon,i} \cdot u_{g,i} = C$, here C increase from 4–12 with particle diameter from 88–369 µm. Considering 94 µm of particle diameter in this work, the C value of 4 is adopted.

Besides, $\rho_{d,i}$ stands for saturated solids carrying capacity of gas, equivalent to solids suspension density at choking [24,25]. In this work, $\rho_{d,i}$ is calculated based on Yang's Equation [25],

$$\frac{2gD_i\left(\varepsilon_{d,i}^{-4.7} - 1\right)}{\left(u_{g,i} - u_t\right)^2} = 6.81 \times 10^5 \frac{\rho_g}{\rho_s} \tag{20}$$

where D_i is the hydraulic diameter of the furnace section of a branch. $\varepsilon_{d,i}$ is choking voidage, also equivalent to the volume fraction of gas when saturated carrying occurs.

Then $\rho_{d,i}$ can be calculated as Equation (21) [23],

$$\rho_{d,i} = \rho_g \varepsilon_{d,i} + \rho_s (1 - \varepsilon_{d,i}) \tag{21}$$

For the reason that the solids concentration in the bottom zone always has a lower value in the center of the furnace and increases towards the wall, $\rho_{a,i}$ can be determined by the modified Patience-Chaouki Equation [26],

$$\frac{\overline{\varepsilon}_a^{0.6} - \varepsilon_{a,i}}{\overline{\varepsilon}_a^{0.6} - \overline{\varepsilon}_a} = 3\left(\frac{r}{R}\right)^4 \tag{22}$$

where r is the horizontal distance to the centerline of the furnace bed width and R equals half bed width in a rectangular cross-section furnace. $\overline{\varepsilon}_a$ is the average voidage at the furnace bottom. $\overline{\rho}_g$ as well as $\rho_{a,i}$ can be calculated similarly to Equation (21) accordingly.

Eventually, solids suspension density at furnace exit $\rho_{e,i}$ can be calculated by equation,

$$\rho_{e,i} = \rho_{d,i} - (\rho_{d,i} - \rho_{a,i})Exp[-a_{\varepsilon,i}(H - h_0)] \tag{23}$$

4.6. Solids Circulation Rates

The solids circulation rate at the standpipe in each recycle loop can be calculated by the following equation [27],

$$G_{sp,i} = \rho_{e,i}(u_{g,i} - u_t)\frac{A_f}{A_{sp}} \tag{24}$$

where u_t is solid terminal velocity. The calculation of u_t is provided in Appendix A.

Furthermore, the average solids circulation rate among four loops at standpipe G_{sp} can be calculated,

$$G_{sp} = \frac{1}{4}\sum_{i=1}^{4} G_{sp,i} \tag{25}$$

4.7. Solution Procedure

With the equations listed above, the furnace solids suspension density distribution and solids circulation rate at standpipe can be determined for each solids recycle loop. They are related to the resistance coefficient of each branch in the connection between cyclones and backpass. Figure 6 gives the solution procedure of the theoretical model.

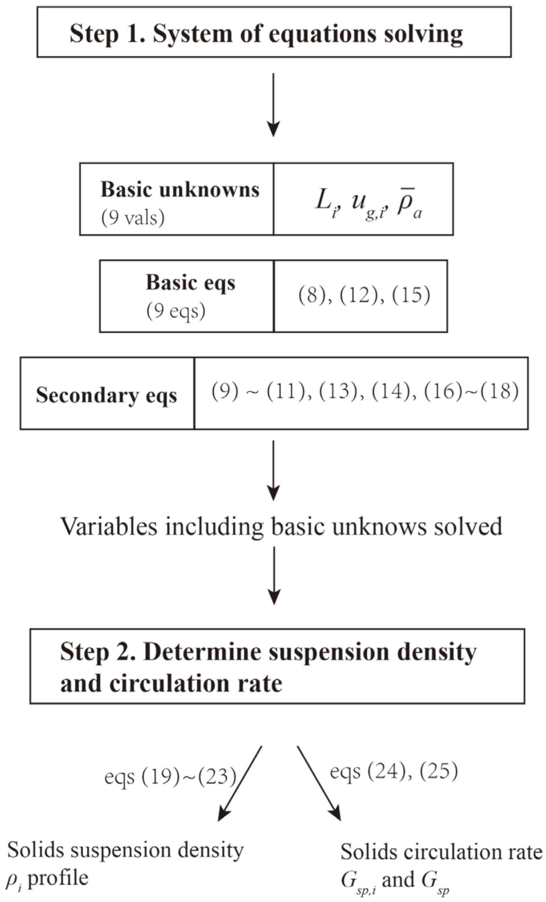

Figure 6. Solution procedure of theoretical calculation.

The calculated value of pressure drops across the furnace, cyclones, and the connection are provided in Appendix B. The experimental data of pressure drops across the furnace and cyclones are also given there.

5. Results and Discussion

5.1. Effect of Overall Resistance Coefficient on Suspension Density Distribution and G_{sp}

Figure 7 shows solids suspension density distribution along with the furnace height with different overall resistance coefficient ξ_{av}, from connection modes including A-type, B-type, and C-type. The theoretical results match well with the experimental data.

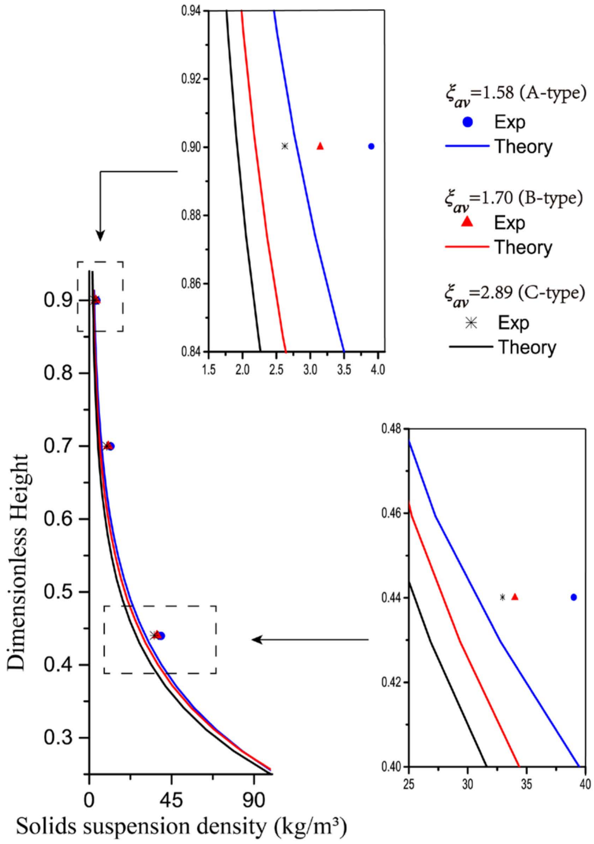

Figure 7. Axial gas-solid suspension density profile at different connection modes.

As mentioned in Section 3.2, the A-type connection mode has the smallest value of overall connection resistance coefficient ξ_{av}. Figure 7 shows the largest suspension density in the furnace above the dense section compared to the other two connections. Besides, the smoothest slope of the suspension density curve along the height of the A-type mode can also be discovered. In contrast, there are fewer solids suspended in the furnace of the B and C-type connection modes, and their suspension density curves along bed height are steeper, reflecting more uneven axial suspension density distribution. This indicates the hydraulic resistance of the connection section affects the solids suspension density distribution in the furnace. Higher pressure resistance of the connection may result in a hindrance curtain at the exit of the furnace so as to prevent the gas-solid up-flowing from the furnace bottom to the top. As a result, the solids suspension density is distributed more non-uniformly in the furnace as ξ_{av} increases.

Figure 8 gives the results of the solids suspension density at specific heights and the average solids circulation rate among standpipes (G_{sp}) with respect to the overall resistance coefficient ξ_{av}. As illustrated in the figure, the solids suspension density in dense phase (ρ_a) of C-type mode is around 30 kg/m^3 larger than that of A-type mode, while the concentration in furnace exit (ρ_e) is 1.8 kg/m^3 less. In terms of average solids circulation rate among four standpipes (G_{sp}), the A-type mode has the largest G_{sp} value of near 100 kg/m^{2}s which is around 20 kg/m^{2}s larger than that of C-type mode.

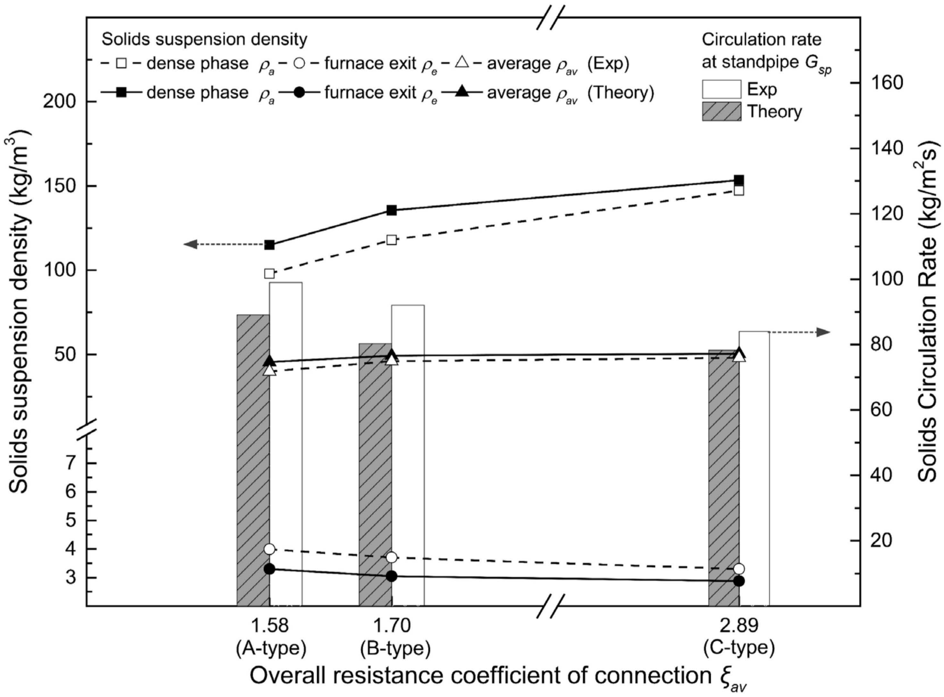

Figure 8. Solids suspension density and G_{sp} in different connection modes.

Sum up with both Figures 7 and 8, ρ_a has the same trend as resistance coefficient ξ_{av} variation, while ρ_e and G_{sp} changes with ξ_{av} reversely. Meanwhile, the average solids suspension densities (ρ_{av}) do not change much for different ξ_{av}.

From those results, it can be deduced that there are more solids transferred from the bottom to the upper furnace when the solids circulation rate increases and the solids circulation is intensified by smaller resistance of a connection. The high circulation rate exerts an effect on larger solids suspension density in the upper dilute zone. Therefore, small ξ_{av} in a connection mode would cause less hindrance for solids circulation and lifting, resulting in better uniformity of axial gas-solid distribution profile.

5.2. Effect of Connection Branch Resistance Distribution on Suspension Density and $G_{sp,i}$

To study the effect of the resistance distribution among connection branches on solids suspension density and the solids circulating rates ($G_{sp,i}$) allocation further, more works were done on C-type connection mode.

The structure of the C-type connection was given in both Figures 4 and 9, there are four exit branch ducts extended from four cyclone outlets. Those ducts compile at different positions successively, forming four connection branches (No. 1–4) for gas flowing from each cyclone outlet to the backpass. As depicted from Figure 9, the resistance coefficients of the connection branches ($\xi_{b,i}$) decrease from branch 1 to 4 as 3.3–2.0, and the value of $\xi_{b,i}$ is smaller if the corresponding branch is closer to backpass.

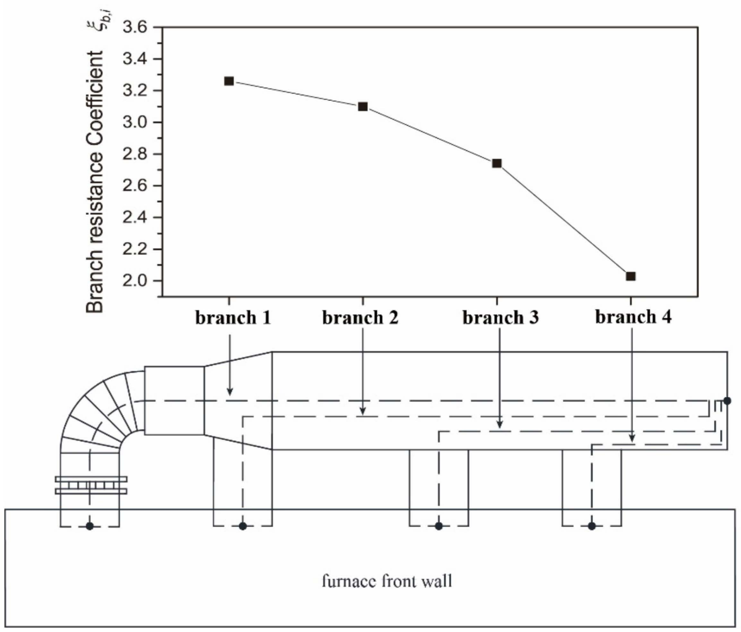

Figure 9. Branch resistance coefficient $\xi_{b,i}$ of C-type connection mode.

Figure 10 gives the solids suspension density distribution on the view of the furnace front wall obtained from the experiments and theoretical calculation. The experimental contour presents the solids suspension density in the furnace from three rows of measuring points (shown in Figure 1b). And the theoretical contour diagram shows the solids suspension density with dimensionless length from 0.2 to 0.8 which corresponding to the theoretical gas-flowing branch 1 to 4 in the furnace, as shown in Figure 5. It can be seen that solids suspension density in the dilute section increases from left to right, with around 3 kg/m^3 variance between branches 1 and 4. And lateral density distribution in the furnace below the transition section (H/h = 0.3–0.5) remains relatively uniform for both experimental and theoretical contours.

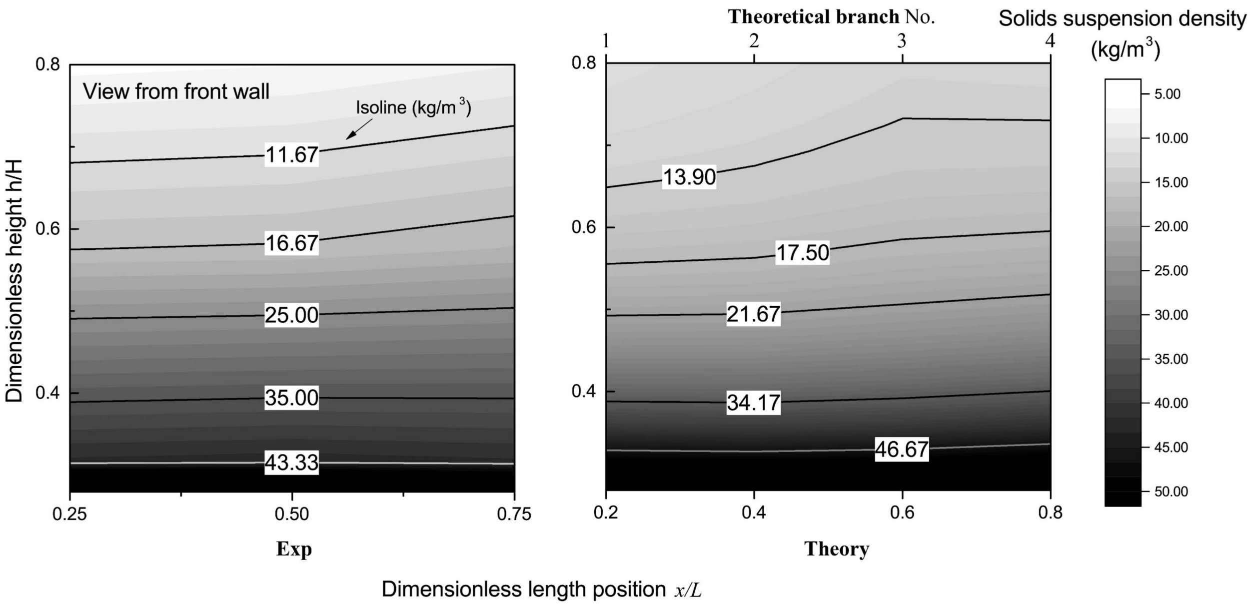

Figure 10. The contour of furnace suspension density of C-type mode.

Figure 11 shows the relationship of standpipe circulation $G_{sp,i}$ distribution among each standpipe, corresponding to each connection branch. Both experimental and theoretical results presented higher $G_{sp,i}$ at lower resistance $\xi_{b,i}$ of a connection branch. To be specific, the circulation rate in branch 4 is the largest and 45 kg/m^{2}s greater than that in branch 1. The relationship between $G_{sp,i,}$ and $\xi_{b,i}$ have a similar trend as solids suspension density in the dilute section in Figure 10.

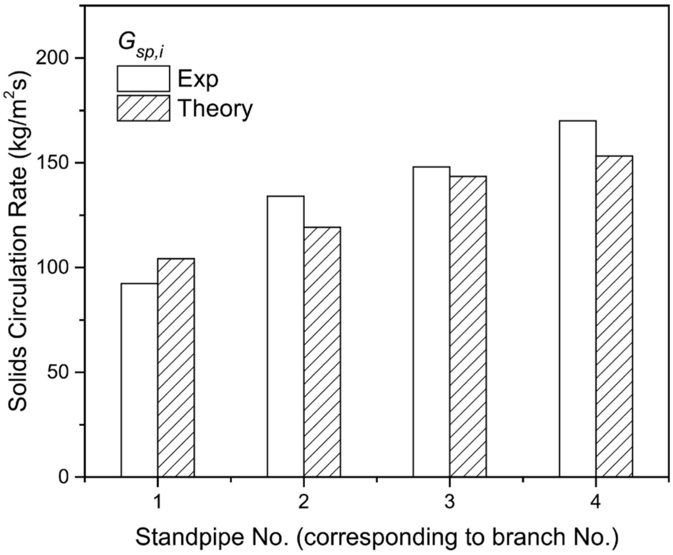

Figure 11. Solids circulation rate of four standpipes of C-type mode (corresponding to four connection branches).

Combined with Figures 10 and 11, it can be summarized that higher $\xi_{b,i}$ of a connection branch may also hinder solids circulation in the corresponding solids recycle loop and consequently reduce furnace solids suspension density in this gas-flowing branch. And the axial solids suspension density distributed more non-uniform with higher $\xi_{b,i}$ of a connection branch.

5.3. Effect of Superficial Velocity on Suspension Density and Circulation Rate

The superficial velocity has a strong impact on furnace solids suspension density distribution, solids circulation rates, and their uniformity. In this section, four different velocity conditions are tested with *Fn* number of 85.2, 91.4, 96.3, 102.5, and corresponding velocities of 0.68, 0.73, 0.78, 0.83 (m/s). The lower limit of the velocity conditions is considering terminal velocity's value of 0.66 m/s that superficial velocity should be larger than that. And the upper limit of 0.83 m/s corresponds to the superficial velocity of the original boiler of 5.26 m/s at 100% Boiler Maximum Continuous Rating (BMCR).

Figure 12 presents the effect of superficial velocity on a solids suspension density on the above furnace dense zone in three connection modes. A smoother curve and larger values of the solids suspension density are achieved when ξ_{av} of a connection mode decreases at all velocities. For different velocity conditions, the axial variance of the solids suspension becomes larger with growing superficial velocity, especially at the lower section.

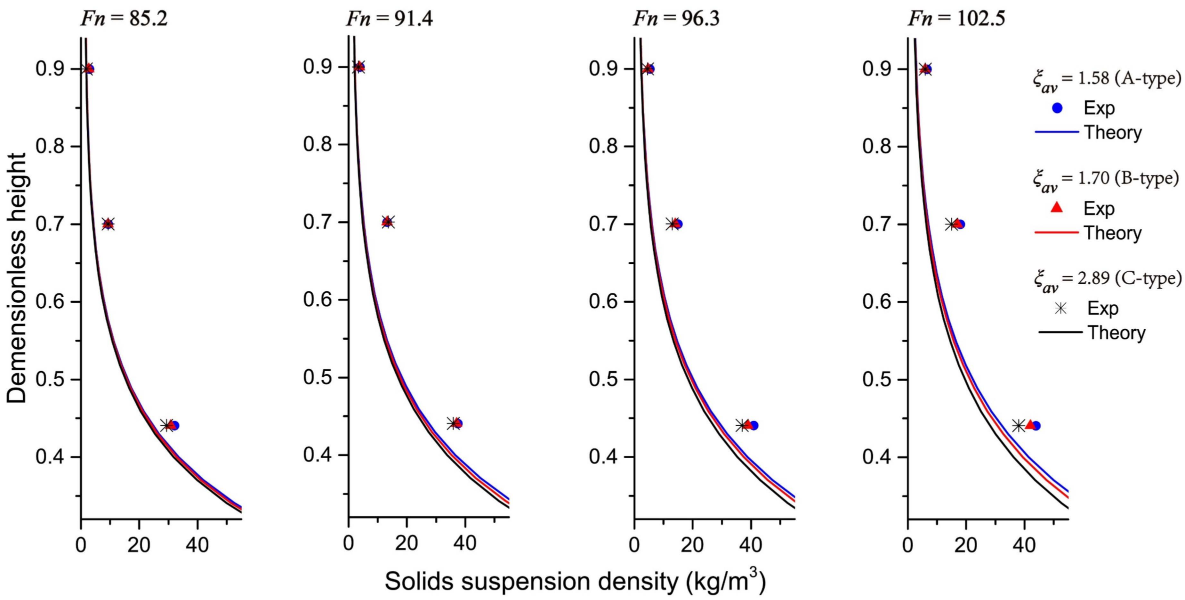

Figure 12. Effect of superficial velocity on suspension density with different ξ_{av}.

Figure 13 gives the effect of superficial velocity on a solids suspension density from C-type connection mode. The No. 4 connection branch, with the smallest resistance coefficient $\xi_{b,i}$, has the largest solids suspension density in the furnace. The suspension density distribution curves show a similar trend with the results from different connection modes in Figure 12. That is, the effect of connection resistance on solids suspension distribution variation can be intensified by increasing superficial velocity. This intensification is most stimulated in the furnace lower section.

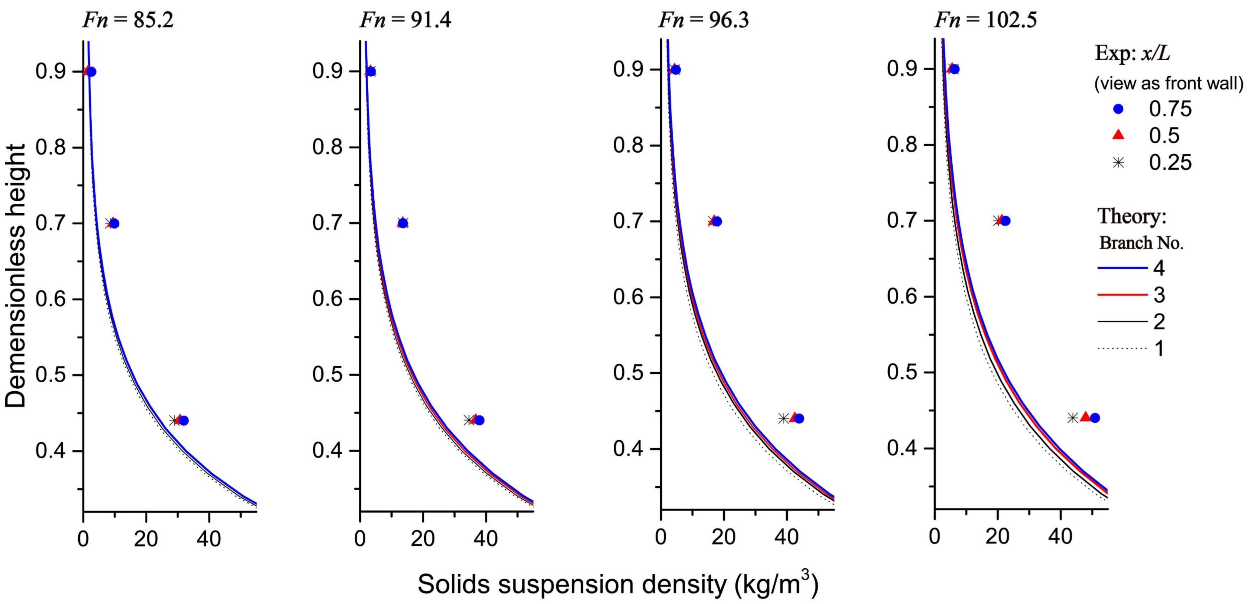

Figure 13. Effect of superficial velocity on solids suspension density (C-type mode).

Figure 14 presents the effect of superficial velocity on solids circulation rates with different ξ_{av}. Both theoretical and experimental results show average circulation rate G_{sp} increases with the superficial velocity in all cases. A circulating system with smaller overall connection resistance ξ_{av} has a larger circulation rate. It can also be depicted from the figure that, for all connection modes, once increasing the superficial velocity, the value of G_{sp} and range of $G_{sp,i}$ among standpipes are enlarged. This indicates higher non-uniformity of $G_{sp,i}$

with increasing superficial velocity. And the velocity effect is most stimulated in C-type mode, probably because of its most uneven $\xi_{b,i}$ distribution.

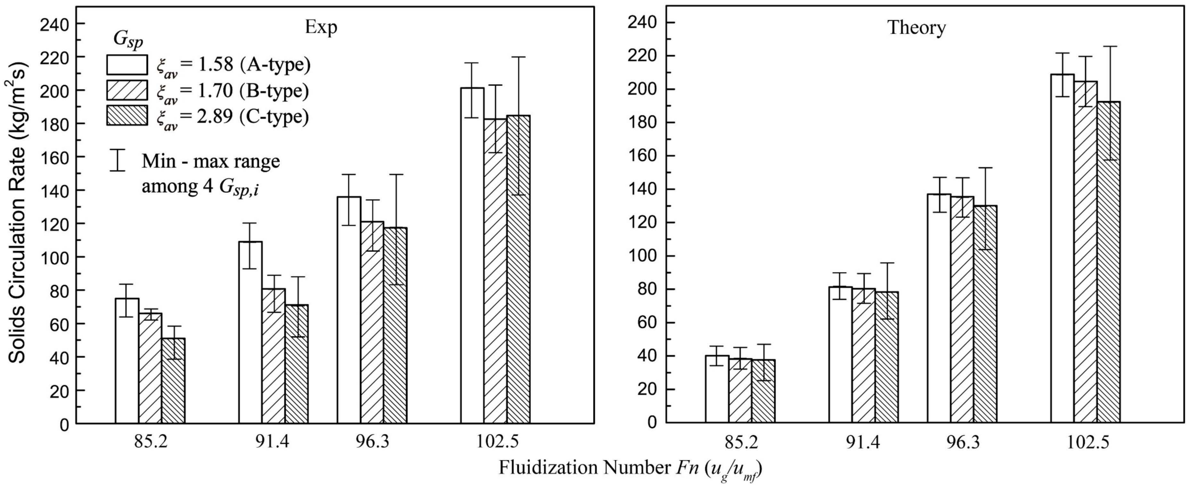

Figure 14. Effect of superficial velocity on solids circulation rate G_{sp} with different ξ_{av}.

The effect of superficial velocity on $G_{sp,i}$ in each solids recycle loop from the C-type connection mode is shown in Figure 15. Increasing superficial velocity intensifies solids circulation rate at all recycle loops. However, this enhancement effect varies with different recycle loops (standpipe No.). The recycle loop with larger corresponding $\xi_{b,i}$ (e.g., No. "1") has slighter changes in circulation rate with superficial velocity. On contrary, the recycle loop No. "4" has the smallest corresponding $\xi_{b,i}$, and its circulation rate increases most enormously with superficial velocity. The different responding effects for superficial velocity among each standpipe can also explain the phenomenon in Figure 14 that, the non-uniformity among $G_{sp,i}$ is enlarged with growing superficial velocity.

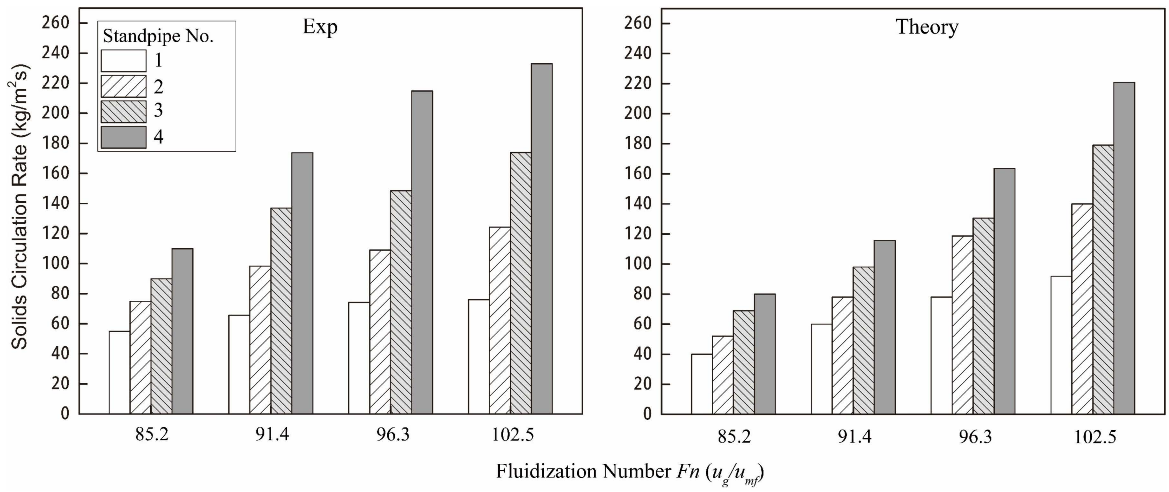

Figure 15. Effect of superficial velocity on $G_{sp,i}$ in each standpipe (C-type mode).

Combined with Figures 12–15, it is apparent that the non-uniformity of furnace solids suspension distribution and solids circulation rate caused by connection resistance is enhanced by superficial velocity. This can be further analyzed that, although ξ_{av} of connection or $\xi_{b,i}$ among branches is constant, the connection pressure drop ($\Delta P_{EF,i}$ in Equation (8) and variation among $\Delta P_{EF,i}$ in different branches are increased by growing velocity. As a result, the furnace gas-solid distribution profile and circulation rates allocation become more uneven with increasing superficial velocity.

6. Conclusions

6.1. The Conclusions for the Investigation

The effect of connection resistance between cyclones and backpass on furnace solids suspension density distribution and solids circulation rates in a multi-cyclone CFB was investigated. The main conclusions are:

(1) The solids suspension density in the furnace and solids circulation rate distributions are influenced by connection resistance. With smaller overall resistance coefficient ξ_{av} of a connection, the axial solids suspension density in the furnace distributes more uniform and solids circulation rate becomes larger;

(2) For branch resistances $\xi_{b,i}$ (i = 1–4) in a connection, smaller $\xi_{b,i}$ leads to higher solids circulation rate in solids recycle loop. Regarding C-type connection mode, the $\xi_{b,i}$ is decreasing from connection branch 1~4, resulting in solids suspension density and circulation rates increasing from corresponding recycle loop 1–4. Smaller $\xi_{b,i}$ of a connection branch also leads to more evenly axial solids suspension density distribution of corresponding recycle loop;

(3) The effect of connection resistance is enhanced by growing superficial velocity. The variance of lateral solids suspension distribution and solids circulation rates allocation becomes larger with higher superficial velocity. For a connection, non-uniformity of branch resistance $\xi_{b,i}$ affects the uneven distribution of solids suspension density and $G_{sp,i}$ allocation among recycling loops, this effect is strongly intensified by growing velocity.

6.2. Suggestions for the Connection Design of Large Scale CFB Boiler

The connection resistance and its distribution between cyclones and backpass should be paid more attention when designing an industry CFB boiler. Some suggestions are given as follows,

(1) It is beneficial to design a simple connection structure with a short distance from cyclones to the backpass. A a small value of overall connection resistance coefficient ξ_{av} should be chosen, for it leads to less resistance for gas-solid circulation and is helpful for operating flexibly.

(2) For each connection branch in a connection mode, the structure and distance from each cyclone to backpass should be close to each other, ensuring uniformity of branch resistance coefficient $\xi_{b,i}$ distribution. It is helpful to diminish uneven solids suspension density distribution and solids circulation rates allocation.

Author Contributions: Conceptualization, G.L. and L.C.; methodology, G.L., L.C., L.L. and W.Z.; validation, L.C., J.W. and X.J.; investigation, G.L., L.C., J.W. and X.J.; resources, W.Z., J.W. and X.J.; writing—original draft preparation, G.L.; writing—review and editing, L.C. and L.L.; funding acquisition, L.C. All authors have read and agreed to the published version of the manuscript.

Funding: This work was supported by the National Key Research & Development Program of China (No. 2020YFB0606201). The program's funder is Ministry of Science and Technology of the People's Republic of China.

Institutional Review Board Statement: Not applicable.

Informed Consent Statement: Not applicable.

Data Availability Statement: Not applicable.

Conflicts of Interest: The authors declare no conflict of interest.

Nomenclature

Symbol	**Explanation**	**Unit**
A_c	Cross-section area of cyclone entrance	m^2
A_{dis}	Cross-section area of non-machanical valve	m^2
A_f	Cross-section area of furnace	m^2
A_{sp}	Cross-section area of standpipe	m^2
Ar	Archimedes number	
D	Width of furnace cross-section	m
d_c	Diameter of cyclone	m
d_s	Diameter of standpipe	m
d_p	Particle diameter	µm
Fn	Fluidization number	-
g	Gravitational constant	m/s^2
G_s	Solids circulation rate	$kg/m^2{\cdot}s$
G_{sf}	Solids circulation rate at furnace	$kg/m^2{\cdot}s$
$G_{sp,i}$	Solids circulation rate at standpipe "*i*"	$kg/m^2{\cdot}s$
G_{sp}	Average solids circulation rate among standpipes	$kg/m^2{\cdot}s$
h_0	Height of dense phase	m
H	Height of furnace	m
H_0	Bed inventory height	m
i	*No.* of theoretical gas branch/solids recycle loop	-
L	Length of furnace cross-section	m
M	Total solids inventory in CFB system	kg
M_{sp}	The mass of solids in standpipe	kg
M_f	The mass of solids in furnace	kg
M_{cyc}	The mass of solids in cyclones	kg
ΔP	Pressure drop	Pa
$\Delta P_{AB,i}$	Pressure drop across furnace of a solids recycle loop	Pa
ΔP_{AB}	Pressure drop across furnace, $\frac{1}{4}\sum \Delta P_{AB,i}$ (i = 1–4)	Pa
$\Delta P_{BE,i}$	Pressure drop across cyclone of a solids recycle loop	Pa
ΔP_{BE}	Pressure drop across cyclones, $\frac{1}{4}\sum \Delta P_{BE,i}$ (i = 1–4)	Pa
$\Delta P_{EF,i}$	Pressure drop across a connection branch	Pa
ΔP_{EF}	Pressure drop across a connection, $\frac{1}{4}\sum \Delta P_{EF,i}$ (i = 1–4)	Pa
$\Delta P_{CD,i}$	Pressure drop across standpipe of a recycle loop	Pa
$\Delta P_{DA,i}$	Pressure drop across loop-seal of a recycle loop	Pa
Re_p	Particle Reynolds number	-
Re_t	Terminal particle Reynolds number	-
u_g	Superficial velocity in furnace	m/s
$u_{g,i}$	Superficial velocity in furnace of a gas flowing branch *i*	m/s
u_{mf}	Minimum fluidized velocity	m/s
u_t	Terminal velocity	m/s
u_{vs}	Air velocity in supply chamber	m/s
u_{vr}	Air velocity in recycle chamber	m/s
ξ_{av}	Overall resistance coefficient of a connection mode	-
$\xi_{b,i}$	Resistance coefficient of connection branch "*i*"	
$\xi_{fr,i}$	Friction resistance coefficient of connection branch "*i*"	-
$\xi_{l,i}$	local resistance coefficient of connection branch "*i*"	
ρ_i	Solids suspension density of a gas flowing branch	kg/m^3
$\rho_{a,i}$	Solids suspension density in dense phase of a gas flowing branch	kg/m^3
$\overline{\rho}_a$	Average solids suspension density in dense phase	kg/m^3
$\rho_{av,i}$	Average solids suspension density above furnace bottom of a branch	kg/m^3
ρ_{av}	Average solids suspension density in furnace	kg/m^3
ρ_b	Particle bulk density	kg/m^3

$\rho_{d,i}$	Saturated carrying capacity of a gas at certain velocity	kg/m^3
$\rho_{e,i}$	Solids suspension density at the furnace exit of a branch	kg/m^3
ρ_e	Average solids suspension density at the furnace exit	kg/m^3
ρ_f	Air density	kg/m^3
ρ_s	Particle density	kg/m^3
ρ_{sus}	Solids suspension density	kg/m^3
ν	Kinetic Viscosity	m^2/s
$\varepsilon_{a,i}$	Voidage at furnace bottom of a branch	–
$\overline{\varepsilon}_a$	Average voidage at furnace bottom	
$\varepsilon_{d,i}$	Saturated solids carrying capacity voidage of a furnace branch	–
ε_{mf}	Minimum fluidized voidage	–
Φ	Sphericity of particle	–

Appendix A. The Calculation of Terminal Velocity

The calculation method for terminal velocity u_t is described in this section. Firstly it is calculated through terminal Reynold number Re_t,

$$Re_t = \frac{u_t d_p}{\nu} \tag{A1}$$

And the terminal particle Reynold number is related to Archimedes number Ar. The calculation differs from various flowing conditions [28],

$$Re_t = \frac{Ar}{18} \qquad \text{Stokes' Law} \qquad (0 < Re_t < 0.4) \tag{A2}$$

$$Re_t = \left(\frac{Ar}{7.5}\right)^{0.666} \qquad \text{Intermediate Law} \qquad (0.4 < Re_t < 500) \tag{A3}$$

$$Re_t = \left(\frac{Ar}{0.33}\right)^{0.5} \qquad \text{Newtons' Law} \qquad (Re_t > 500) \tag{A4}$$

Here the Archimedes number can be expressed as,

$$Ar = \frac{d_p^3 g \rho_f \left(\rho_s - \rho_f\right)}{\mu^2} \tag{A5}$$

where μ is the dynamic viscosity of fluid and $\mu = \nu\rho_f$.

In this study, the value of d_p, ν, ρ_s, etc. can be found in Table 1. The calculated results of u_t and Re_t are equaled to 0.66 m/s and 3.2, respectively, corresponding to the “Intermediate Law”.

Appendix B. The Pressure Drop Across Furnace, Cyclones and The Connections

The pressure drops across furnace (ΔP_{AB}) and cyclones (ΔP_{BE}) were recorded during the experiments with A, B, and C-type connection modes. The data is listed in Table A1. Meanwhile, Table A2 gives the calculated pressure drops of furnace, cyclones, and connections (ΔP_{EF}).

It needs to notice that for Table A1, ΔP_{AB} is calculated by averaging the pressure drops of three measuring rows, while for Table A2 it is the average value of four theoretical solids recycle loops $\Delta P_{AB} = \frac{1}{4}\sum \Delta P_{AB,i}$ (i = 1–4). The same methods are applied in ΔP_{BE} and ΔP_{EF}.

Table A1. Pressure drop across furnace and cyclones (Exp. unit of Pa).

Type of Connection Modes	ΔP_{AB}	ΔP_{BE}
A-type	595.9	63.2
B-type	645.2	66.4
C-type	661.6	65.2

Table A2. Pressure drop across furnace, cyclones, and connection (Theory, unit of Pa).

Type of Connection Modes	ΔP_{AB}	ΔP_{BE}	ΔP_{EF}
A-type	604.6	57.1	32.4
B-type	653.2	57.5	38.2
C-type	667.1	58.2	49.5

References

1. Zhou, X.L.; Cheng, L.M.; Zhang, J.; Wang, Q.H.; Luo, Z.Y.; Cen, K.F. Experimental Study on Solids Suspension Density and Solids Circulating Rate in a CFB with Six Circulating Loops. *Proc. CSEE* **2012**, *32*, 31–36.
2. Wang, F.J.; Song, G.L.; Wang, X.F.; Liu, Z.C.; Sun, Y.K.; Lu, Q.G. Cold Experimental Study on a CFB with Four Cyclone Separators on the Same Side. *Power Syst. Eng.* **2014**, *3*, 17–19.
3. Lee, J.M.; Kim, J.S.; Kim, J.J. Characteristics of Solid Hold Up and Circulation Rate in the CFB Reactor with 3-Loops. *Korean J. Chem. Eng.* **2001**, *18*, 1000–1004. [CrossRef]
4. Yang, S.; Yang, H.R.; Liu, Q.; Zhang, H.; Wu, Y.X.; Yue, G.X.; Wang, Y.Z. Research on Flow Non-Uniformity in Main Circulation Loop of a CFB Boiler with Multiple Cyclones. In Proceedings of the 20th International Conference on Fluidized Bed Combustion, Xi'an, China, 18–21 May 2009; Springer: Berlin/Heidelberg, Germany, 2009; Volume 139, pp. 341–344.
5. Zheng, W.J.; Zhang, M.; Zhang, Y.; Lyu, J.F.; Yang, H.R. The effect of the secondary air injection on the gas-solid flow characteristics in the circulating fluidized bed. *Chem. Eng. Res. Des.* **2019**, *141*, 220–228. [CrossRef]
6. Karlsson, T.; Liu, X.; Pallarès, D.; Johnsson, F. Solids circulation in circulating fluidized beds with low riser aspect ratio and varying total solids inventory. *Powder Technol.* **2017**, *316*, 670–676. [CrossRef]
7. Mo, X.; Cai, R.X.; Huang, X.D.; Zhang, M.; Yang, H.R. The effects of wall friction and solid acceleration on the mal-distribution of gas-solid flow in double identical parallel cyclones. *Powder Technol.* **2015**, *286*, 471–477. [CrossRef]
8. Harris, A.T.; Davidson, J.F.; Thorpe, R.B. Influence of exit geometry in circulating fluidized-bed risers. *AIChE J.* **2003**, *49*, 52–64. [CrossRef]
9. Wang, S.; Luo, K.; Hu, C.S.; Fan, J.R. CFD-DEM study of the effect of cyclone arrangements on the gas-solid flow dynamics in the full-loop circulating fluidized bed. *Chem. Eng. Sci.* **2017**, *172*, 199–215. [CrossRef]
10. Knowlton, T.M. Standpipes and return systems. In *Circulating Fluidized Beds*; Springer: Dordrecht, The Netherlands, 1997; pp. 214–260.
11. Sun, X.B.; Li, G.H.; Jiang, M.H. Study on Several Forward Tasks in the Technical Sector of CFB Boilers. *Therm. Power Gener.* **2005**, *34*, 1–5.
12. Song, G.L.; Yang, Z.; Zhou, T.; Lyu, Q.G. Operating technical characteristics on asymmetrical arrangement of six cyclones in a 600 MW supercritical CFB boiler. *Appl. Therm. Eng.* **2018**, *143*, 236–247. [CrossRef]
13. Mo, X.; Cai, R.X.; Lyu, J.F. Analysis of Non-uniform Distribution of Gas-Solid Flow in the 600 MW(e) CFB Boiler Based on the Non-uniform Distribution of Returning Ash Temperature. *Proc. CSEE* **2016**, *36*, 153–158.
14. Glicksman, L.R. Scaling relationships for fluidized beds. *Chem. Eng. Sci.* **1984**, *39*, 1373–1379. [CrossRef]
15. Glicksman, L.R. Scaling relationships for fluidized beds. *Chem. Eng. Sci.* **1988**, *43*, 1419–1421. [CrossRef]
16. Idelcik, I.E.; Ginevskiy, A.S.; Kolesnikov, A.V. *Handbook of Hydraulic Resistance*; Hemisphere Publishing Corp.: Washington, DC, USA, 1986.
17. Zheng, Y.; Lu, X.F.; Yang, W.Q.; Fan, L.Y.; Wang, Q.H.; Yan, J. Simulation of Particle Concentration Distribution in a Large-scale Circulating Fluidized Bed Boiler at Different Material-returning Deviations. *Proc. CSEE* **2020**, *40*, 848–858.
18. Bi, H.; Zhu, J.X. Static instability analysis of circulating fluidized beds and concept of high-density risers. *AIChE J.* **1993**, *39*, 1272–1280. [CrossRef]
19. Shepherd, C.B.; Lapple, C.E. Flow Pattern and Pressure Drop. *Ind. Eng. Chem.* **1939**, *31*, 972–984. [CrossRef]
20. Chen, H.Z.; Yang, D.W.; Li, H.Z.; Tan, S.Y. Study on the overall pressure balance of a downflow circulating fluidized bed system. *China Particuology* **2006**, *4*, 153–159. [CrossRef]
21. Rhodes, M.J.; Geldart, D. A model for the circulating fluidized bed. *Powder Technol.* **1987**, *53*, 155–162. [CrossRef]
22. Bai, D.; Issangya, A.S.; Zhu, J.X.; Grace, J.R. Analysis of the Overall Pressure Balance around a High-Density Circulating Fluidized Bed. *Ind. Eng. Chem. Res.* **1997**, *36*, 3898–3903. [CrossRef]

23. Kunii, D.; Levenspiel, O. Entrainment of solids from fluidized beds I. Hold-up of solids in the freeboard II. Operation of fast fluidized beds. *Powder Technol.* **1990**, *61*, 193–206. [CrossRef]
24. Basu, P. *Circulating Fluidized Bed Boilers*; Springer International Publishing: Cham, Switzerland, 2015; Volume 54, ISBN 978-3-319-06172-6.
25. Yang, W.C. Criteria for choking in vertical pneumatic conveying lines. *Powder Technol.* **1983**, *35*, 143–150. [CrossRef]
26. Schlichthaerle, P.; Werther, J. Axial pressure profiles and solids concentration distributions in the CFB bottom zone. *Chem. Eng. Sci.* **1999**, *54*, 5485–5493. [CrossRef]
27. Stollhof, M.; Penthor, S.; Mayer, K.; Hofbauer, H. Estimation of the solid circulation rate in circulating fluidized bed systems. *Powder Technol.* **2018**, *336*, 1–11. [CrossRef]
28. Howard, J.R. *Fluidized Bed Technology—Principles and Applications*; CRC Press: Bristol, UK, 1989.